The UVISI Instrument

Kevin J. Heffernan, John E. Heiss, John D. Boldt, E. Hugo Darlington, Keith Peacock, Terry J. Harris, and Mark J. Mayr

The Ultraviolet and Visible Imagers and Spectrographic Imagers (UVISI) instrument is a complex of nine sensor units (five spectrographic imagers and four imagers) and multiple processors that will provide detailed images and spectra of targets for the Midcourse Space Experiment mission. Imaging and spectroscopy each cover the range from 110 nm (far ultraviolet) to 900 nm (near infrared). UVISI is intended to investigate a multitude of celestial, atmospheric, and point sources over its planned 4-year lifetime. At 104 W and 211 kg, it is not only the largest free-flying instrument ever built at APL, but is also larger than 47 of the 55 APL-built spacecraft and more complex than many of them. This article discusses the specifications of UVISI and its hardware and software features. It also attempts to give the reader a sense of the design trade-offs made during UVISI development that resulted in its present configuration.

INTRODUCTION

The Ultraviolet and Visible Imagers and Spectrographic Imagers (UVISI) instrument is a hyperspectral remote sensing instrument[1] designed to investigate a variety of military, scientific, and environmental targets for the Midcourse Space Experiment (MSX) mission. It consists of five spectrographic imagers (SPIMs), four imagers, and a set of instrument electronics (Fig. 1) that provide control functions and image processing capabilities. It is designed to provide simultaneous multispectral characterization of upper and meso atmospheres and celestial backgrounds in the range from 110 to 900 nm.

The five SPIMs will yield full spatial images of various objects and backgrounds. Each pixel of an image will have 272 spectral bands. Primary observations for the SPIMs include terrestrial dayglow and nightglow, auroral radiance, stellar and zodiacal light spectra, and plume contrails in the upper atmosphere. When suitably inverted, the spectral radiances of the airglow reveal concentrations of major and minor atmospheric constituents (including species such as O_2, N_2, NO, OH, and O_3), their temperature and altitude profiles, etc. Spectrographic investigation of the aurora provides estimates of the fluxes and energies of the
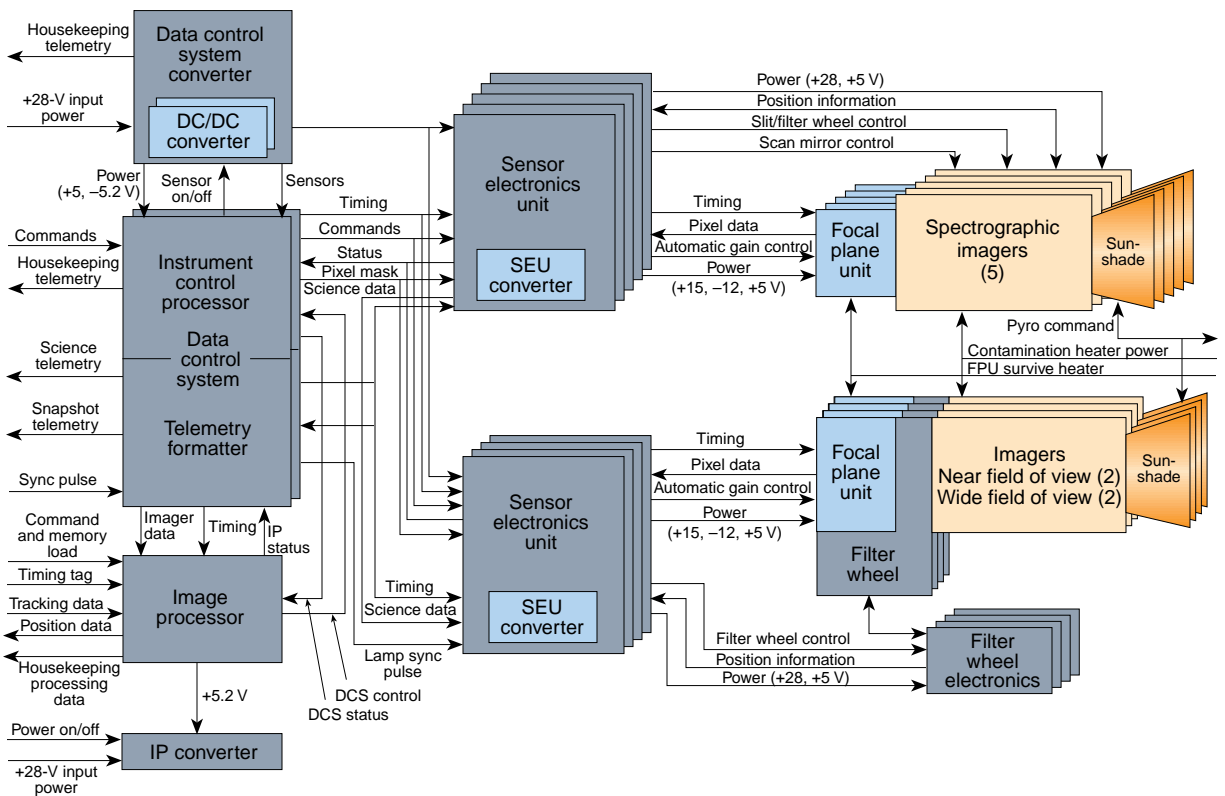
Figure 1. UVISI instrument block diagram (IP, image processor; SEU, sensor electronics unit; FPU, focal plane unit; DCS, data control system).

precipitating charged particles that cause the aurora, which in turn yields information about the ionospheric and magnetospheric disturbances that occur during geomagnetic storms. In astronomy, the SPIMs will measure the diffuse ultraviolet background of the sky. The four UVISI imagers will produce both wide- and narrow-field-of-view (FOV) images of point sources such as stars and extended sources such as aurora. The higher time and spatial resolution of the imager observations will complement those of the SPIMs.[2]

All nine sensors are mounted on the periphery of the instrument (upper) section of the MSX spacecraft. They are coaligned with themselves as well as with the Spatial Infrared Imaging Telescope III (SPIRIT III), the Space-Based Visible sensor, and the Contamination Experiment instruments. The core instrument electronics are located on the lower section of the spacecraft. Figure 2 shows the location of the UVISI hardware. Two of the UVISI sensors—the wide-FOV imager and SPIM 3—serve as detectors in support of the Contamination Experiment's particulate and water vapor investigations. These two are mounted so that their FOVs intersect the beams of the experiment's xenon and krypton lamps, respectively.

The five SPIMs use an off-axis Wadsworth folded optical configuration for compactness, which also minimizes the number of surface reflections required in the far ultraviolet. Selectable slit widths provide instantaneous FOVs of $0.05 \times 1.0°$ or $0.1 \times 1.0°$. The $1.0°$ slit length is divided into 40 spatial pixels, each separated into 272 spectral components. Thus, the SPIM pixels are $0.025 \times 0.05°$ or $0.025 \times 0.1°$. A full image is built up by scanning the FOV using a pivoted telescope mirror. The resulting sensor field of regard for a full spectral image is $1.0 \times 1.0°$. The SPIMs have spectral resolutions ranging from 0.5 to 4.0 nm depending on wavelength and data mode. Time resolutions for a full $1 \times 1°$ spectrographic image can be varied from 5 to 20 s, depending on the selected slit width and frame rate.

Two of the four imagers provide ultraviolet imaging capability; the other two are sensitive in the visible. One each of the ultraviolet and visible imagers has a narrow FOV of $1.59 \times 1.28°$. The other two have a wide FOV of $13.1 \times 10.5°$, which is about an order of magnitude larger. Three different optical designs were used for the four imagers. Each imager has a six-position filter wheel. In addition to the "closed" and "open" positions, each wheel has a neutral density filter to extend the imagers' dynamic ranges and several narrowband filters for specific scientific investigations. The imagers have time resolutions of 0.5 s for a full image or 0.25 s for an image that covers 50% of the FOV. Spatial resolutions are 108×92 μrad for the narrowFOV and 890×716 μrad for the wide-FOV imagers.

Figure 3 details the spectral coverage of each of the SPIMs and imagers.

The nine sensors all employ intensified charge-coupled device (CCD) detectors located in the focal plane unit (FPU). FPUs for each sensor are identical, with the exception of the intensifier photocathode material selected on the basis of the bandpass of interest. The sensors have an intrascene dynamic range of 10^3 and an interscene dynamic range between 10^8 and 10^{10}. The former is limited by the analog-to-digital converters, whereas the total range consists of various combinations of the variable intensifier gain (10^3) and gate (500), the neutral density filters (10^2 to 10^4), and the analog-to-digital converter (10^3). Each sensor has a sunshade/baffle with a nonreclosable door and a sensor electronics unit (SEU). The SEU is a dedicated microcomputer that provides control, communications, data formatting, and power conversion for each sensor.

The entire UVISI instrument is controlled by a central processor and control assembly called the data control system (DCS), which provides command reception and implementation, science and status data formatting, and communications capabilities with the spacecraft, the sensors, and the image processor. Power conversion for the DCS, power switching for the sensors, and the current monitoring capability are performed in the DCS converter (DCSC).
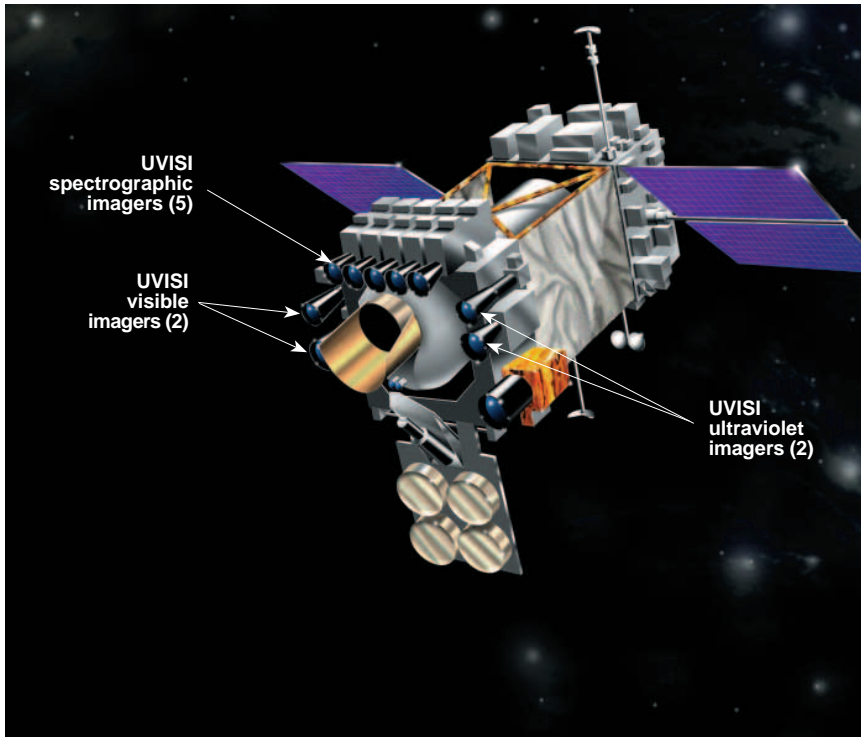

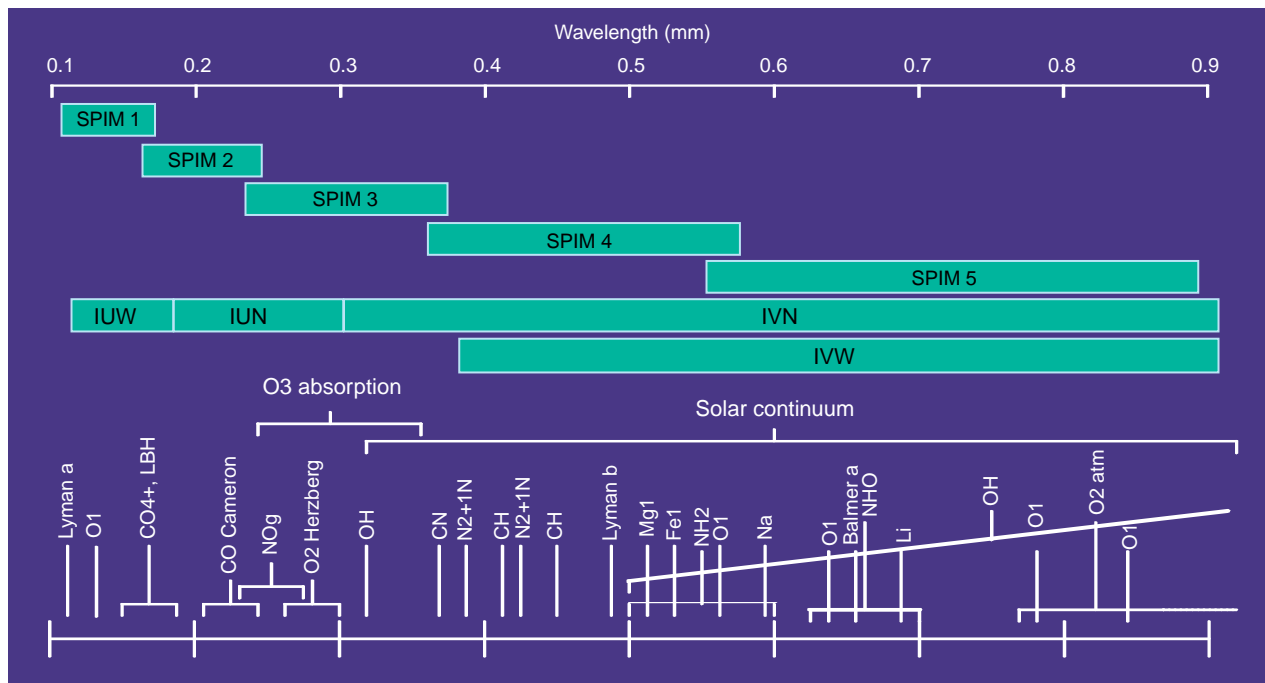**Figure 2**. MSX spacecraft layout showing location of UVISI sensors.

Figure 3. UVISI wavelength coverage. Notations at bottom of figure represent spectral lines of various atomic and molecular components expected to be analyzed. (SPIM = spectrographic imager; IUW and IUN = wide- and narrow-FOV ultraviolet imagers, respectively; IVW and IVN = wide- and narrow-FOV visible imagers, respectively.)

The image processor is a separate assembly that can analyze images in real time. Data from a single imager can be directed to the image processor to be searched for potential targets. The image processor processes each image, forms a prioritized list of possible targets, and forwards the list, locations, and several other parameters to the tracking processor as part of the tracking control loop.

UVISI was developed with three precepts in mind: robustness, maximum use of common designs, and flexibility. Two approaches were taken to minimize single point failures. Redundancy was used for the core instrument-level electronics, the DCS, and the DCSC; a distributed processing and power system philosophy was adopted for the sensors. Each of the nine sensors, for example, has its own microprocessor-based controller (SEU) and DC/DC converter. A failure in a single sensor will not affect the other eight.

The nine onboard sensors provided a unique opportunity to maximize the use of common designs. Commonality exists at various levels in the FPUs, SEUs, sunshades, spectrographic imager optics/housings, narrow-FOV imager, DCS, DCSC, and image processor designs. This approach greatly reduces the development cost of the instrument while maximizing reliability with little reduction in capability.

UVISI was designed to be extremely flexible so that it could handle a variety of target sizes, irradiances, and spectral ranges; take maximum advantage of spacecraft resources; increase failure recovery options; and maximize visibility for troubleshooting. We present numerous examples of both commonality and flexibility throughout this article.

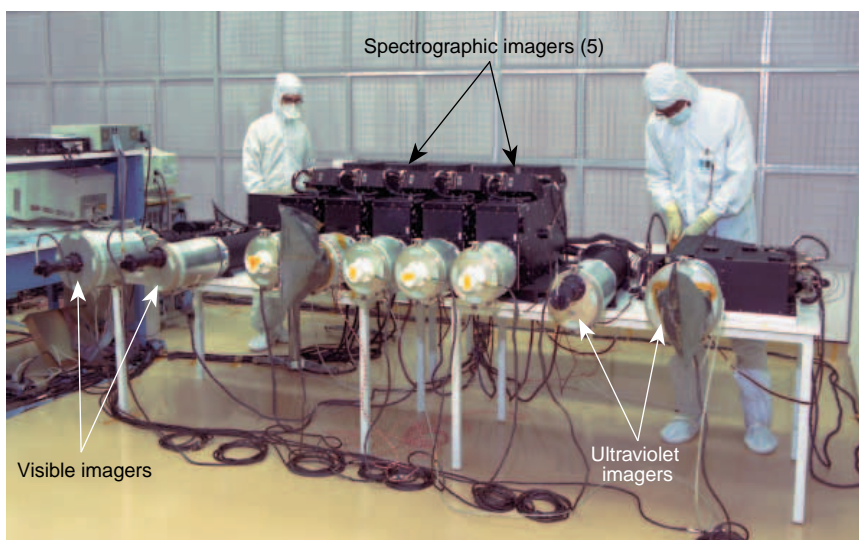Figure 4 is a photograph of UVISI taken in the clean room during instrument-level integration. It will help orient the reader as to the size and appearance of the instrument's various sensor and electronics assemblies.

SENSORS

Spectrographic Imagers

The five SPIMs cover overlapping segments of the spectral range from 110 to 900 nm. The grating for each was selected to obtain identical optical layouts with a spectral range of ≈1.8:1 in wavelength and 2 to 4% spectral overlap for each sensor. Grating, optical coatings, slit filter, and photocathode material determine sensor responsivity. Table 1 presents details of the SPIM design and performance characteristics.[3] The short-wavelength end of the spectrum is determined by the transmissive optical materials. Magnesium fluoride, the most suitable material for the shortest wavelengths, cuts off at around 115 nm. The long-wavelength limit is determined by declining photocathode response.

The SPIM optical layout is shown in Fig. 5. We selected an off-axis Wadsworth configuration with a spherical diffraction grating that provides both dispersion and imaging to attain the best compromise among design complexity, number of components, package size, and optical efficiency. At the short wavelengths, the reflective coatings have low efficiency, making it desirable to reduce the number of reflections. The SPIM optics/housing assembly weighs 9.5 kg. With the FPU, SEU, and sunshade attached, the complete sensor is 80.3 × 23.1 × 43.9 cm (length, width, and height, respectively, throughout the article), weighs 15.8 kg, and dissipates 10.3 W of power.

The telescope mirror is an off-axis parabola with a clear aperture of 120 mm and the ability to view a 1.2 × 1.2° scene. It images the scene onto the entrance slit with insignificant aberrations. The slit selects the area of the scene that will be imaged onto the FPU detector and eliminates the rest of the field. Two different slit sizes are used, 1.2 × 0.1° and 1.2 × 0.05°. The slit length is divided into 48 spatial pixels (spatial resolution of 0.025 × 0.05°), of which only 40 are used. Each spatial pixel is divided into 272 spectral bins. The telescope mirror is rotated about an axis parallel to the length of the slit, thereby altering the portion of the scene that is imaged onto the slit. The minimum mirror movement is 0.025° which, because the rotation angle is doubled by the reflection, results in an image movement of 0.05° (the

Figure 4. The UVISI instrument during integrated bench testing in a class 10,000 clean room. Test lamps are attached to each sensor. Bags with purge gas enhance the spectrum in the ultraviolet. Electronics are located behind the visible imagers.

Table 1. UVISI predicted performance characteristics: spectrographic imagers (SPIMs).

	SPIM 1	SPIM 2	SPIM 3	SPIM 4	SPIM 5
Field of view (deg)	0.05×1.0	0.05×1.0	0.05×1.0	0.5×1.0	0.05×1.0
	or	or	or	or	or
	0.1×1.0	0.1×1.0	0.1×1.0	0.1×1.0	0.1×1.0
Spectral range (nm)	110–170	162–252	251–384	378–584	580–893
Slit 1	0.1° open	0.1° open	0.05° open	0.1° open	0.1° open
Slit 2	0.05° open	0.05° BP[a]	0.05° BP[a]	0.05° open	0.05° open
Slit 3	0.1°, BaF[b]	0.1°, ND2[c]	0.1°, ND2[c]	0.1°, ND2[c]	0.1°, ND2[c]
Slit 4	0.05°, BaF[b]	0.05°, ND2[c]	0.05°, ND2[c]	0.05°, ND2[c]	0.05°, ND2[c]
Slit 5	Closed	Closed	Closed	Closed	Closed
Sensitivity estimate[d] (photons/cm^2·s)	5	2	3	1	1
Window	MgF_2	MgF_2	SiO_2	SiO_2	SiO_2
Photocathode	CsI	RbTe	KCsSb (bialkali)	Extended S20	Extended S20
Spatial resolution (mrad)	0.44	0.44	0.44	0.44	0.44
Spectral resolution (nm) 0.10° slit/0.05° slit	0.8/0.5	1.2/0.9	1.8/1.5	2.8/2.1	4.3/2.9
Collecting area (cm^2)	110	110	110	110	110
Grating ruling (lines/mm)	2571	1714	1125	739	480

[a]BP = bandpass filters: SPIM 2, 220-nm center; SPIM 3, 260-nm center.
[b]BaF = barium fluoride filter.
[c]ND = neutral density filter.
[d]Predicted sensitivity for wide, open slit position.

minimum slit width). The two-dimensional spatial image is built up by rotating the telescope mirror, so that the image is shifted by the width of the slit on consecutive frames. The maximum image movement is ±0.6° which, together with the slit length, results in the $1.2 \times 1.2°$ scene. The actual field of regard used is 1.0 $\times$ 1.0°, and it can be adjusted anywhere within the scene to correct for misalignments of the five SPIMs.

The SPIMs are nominally operated at a 2-Hz frame rate with a 4-Hz option. Depending on frame rate and slit size, a $1.0 \times 1.0°$ image can be formed in 2.5 s (4 Hz, 0.1° slit width) to 10 s (2 Hz, 0.05° slit width).

The collimator mirror is an off-axis parabola with a focal length of about 333 mm and an off-axis distance of 71 mm. It collimates the diverging beam from the slit and images the aperture stop (the telescope mirror) at the grating. These operations minimize the size of the grating and ensure that the mask around the grating prevents stray light.

The diffraction grating reflects and disperses the incident light. There are two factors to consider in grating design: the wavelength range to be spread across the detector and the central wavelength of that range. These are controlled by two variables, the incident angle at
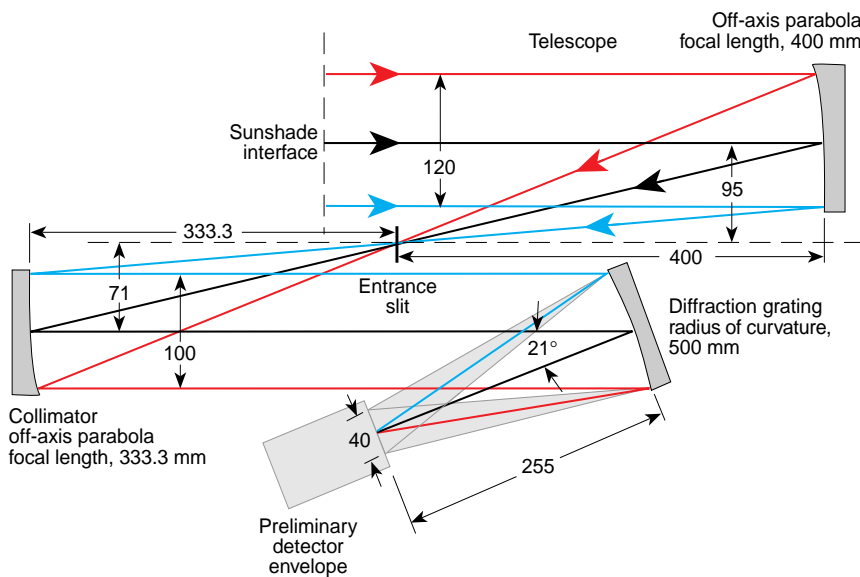

Figure 5. Spectrographic imager optical layout. Dimensions are in millimeters.

the grating and the line width of the ruling. The central wavelength is diffracted along the grating normal so that the diffraction angle is not a variable.[3] Table 1 lists the rulings that give the required dispersions. The final image produced is free of astigmatism on axis at the central wavelength.

The SPIMs are designed to operate over the temperature range of -30 to $-10°C$. They are initially focused and aligned, however, at room temperature. To minimize focus shifts due to bulk temperature changes, both the housing and the optics are made of aluminum. Several optical coatings including MgF_2, SiO_2, and gold are used for the various optical components.

To reduce costs, the scan mirror, the slit mechanisms, as well as the imager filter wheels are designed to use the same variable reluctance stepper motor with a 15° step size and identical motor drive electronics. The mirror is cam-driven, whereas the slit and filter wheels employ geneva mechanisms.

In operation, the angular step size of the scan mirror is commandable, the default being half of the current slit width. For flexibility, the scan range, center position, and number of frames to dwell at each position are all variables. The SPIMs can be operated synchronously or independently, or they can be set to stare if required.

The slit mechanisms have five positions, 0.05 and 0.1° open, 0.05 and 0.1° with neutral density 2.0 filters, and a closed position. The shortest-wavelength sensor, SPIM 1, contains a barium fluoride filter instead of the neutral density filter to provide attenuation of the spectrum below 130 nm. This feature eliminates the strong hydrogen Lyman α emission at 121.6 nm of the geocorona. For similar reasons, a filter was added to the 0.05° open slit position on SPIM 2 to increase the out-of-band rejection on the long-wavelength end and in SPIM 3 to reduce the in-band dynamic range. Short-wavelength cutoff filters are included after the slit to eliminate the higher-order spectral bands in SPIMs 2 through 5.

The maximum spatial resolution of a SPIM is 0.025° (40 pixels over a 1.0° slit width). Each spatial pixel is divided into a maximum of 272 spectral bins. Maximum spectral resolutions vary from 0.5 nm (SPIM 1) to 4 nm (SPIM 5). A temporal resolution option of 0.25 or 0.5 s is available as well. Spatial pixels can be summed by 2, 4, or 8 to form superpixels. Similarly, spec-tral bins can be summed by 2 or 4 to form superbins. Spatial, spectral, and temporal resolutions can be traded off in powers of 2 to make the most efficient use of the available data rate for each specific experiment.

Imagers

As with the SPIMs, the total spectral range for imaging is 110 to 900 nm. The mission and science requirements call for large FOV coverage in some spectral regions and high spatial resolution in others. Two of the imagers have narrow FOVs and two have wide FOVs. Unlike the SPIMs, the four imagers do not all have the same optical and mechanical designs; three of the four designs are unique (see Table 2).

The two narrow-FOV imagers have reflective telescopes with nearly identical optical and mechanical designs, differing primarily in their spectral coverage. The narrow-FOV ultraviolet and visible imagers operate from 180 to 300 nm and 300 to 900 nm, respectively. The key design differences between the two are the photocathode materials in the image intensifier and the choice of spectral filters. The spatial resolution of about 0.1 mrad was selected to be commensurate with the resolution of SPIRIT III.

The two wide-FOV imagers have different optical and mechanical designs but similar large FOVs (approximately $10.5 \times 13.1°$). The wide-FOV ultraviolet imager operates from 110 to 180 nm. A reflective off-axis telescope design was selected to simultaneously

Table 2. UVISI predicted performance characteristics: imagers.

	Narrow-FOV ultraviolet imager	Wide-FOV ultraviolet imager	Narrow-FOV visible imager	Wide-FOV visible imager
Field of view (deg)	1.6×1.3	13.1×10.5	1.6×1.3	13.1×10.5
Filter 1 (nm)	Closed	Closed	Closed	Closed
Filter 2 (nm)	180–300, ND3[a]	110–180, ND3[a]	300–900, ND4[a]	380–900, ND4[a]
Filter 3 (nm)	230–260	128–138	350–440	529–631
Filter 4 (nm)	180–300	110–180	300–900	380–900
Filter 5 (nm)	200–230	117–127	305–315	426–429
Filter 6 (nm)	260–300, polarized	145–180	470–640	380–900, near focus
Sensitivity estimate[b] (photons/cm^2·s)	2	5	1	6
Window	MgF_2	MgF_2	SiO_2	SiO_2
Photocathode	RbTe	CsI	Extended S20	Extended S20
Spatial resolution (mrad)	0.11	0.89	0.11	0.89
Collecting area (cm^2)	130	25	130	25

[a]ND = neutral density filter.
[b]Predicted sensitivity for wide, open filter position.

achieve high throughput in the far ultraviolet, wide FOV, and high resolution. The wide-FOV visible imager operates within the 400- to 900-nm spectral band. The availability of suitable transmissive glasses in the visible spectral range allowed us to use a refractive imager design, thereby saving considerable weight, volume, and cost.

Common Imager Design Elements

As mentioned earlier, all nine UVISI sensors use common FPU and SEU designs. Each of the four imagers also uses a common filter wheel design. The filter wheels have six positions including five transmissive elements and one opaque or closed position. The five transmissive elements consist of one broad spectral band (open) filter, one neutral density (broad spectral band with transmission reduced by 10^n) filter, and typically three narrow spectral bandpass filters. The SEU monitors wheel position and develops commands for the stepper motor, which drives the filter wheel via a gear train and geneva mechanism.

Environmental conditions dictated many of the material choices in the imager designs. We used radiation-resistant glass in both the wide-FOV visible lenses and in the substrates of the spectral filters. The MSX orbit will expose UVISI to a mission radiation level of 15 krad (Si) for a total dose that was confirmed by modeling.[4] Under these conditions, normal optical glass will become discolored or cloudy.[5] Measurements made at APL on irradiated, normal, high-index glass show markedly reduced transmission after 10 krad of gamma radiation.[6] The use of radiation-resistant optical glass stabilized with cerium doping largely eliminates radiation damage.[7]

Because the flight operating temperature range for each imager is significantly lower than room temperature, we needed an opto-mechanical design immune to misalignments from bulk temperature change. For the compact refractive wide-FOV visible design, ample tolerances alone afforded such immunity. For the three reflective imagers, however, an all-aluminum (mirrors, mounts, and structure) design allowed spacing changes between the mirrors caused by bulk temperature changes to be precisely compensated by corresponding changes in the radii of curvature of the mirrors.

The mirrors were constructed by machining the aluminum part close to the desired curvature. A coating of electroless nickel several thousandths of an inch thick was applied to the surface and was then ground and polished to the final surface figure. The appropriate reflective coating was then applied to the nickel. The grinding and polishing procedure is similar to that required for a glass mirror, except that working metal mirrors to tight figure tolerances is more difficult and time-consuming. An advantage of metal mirrors, however, is that the three mounting tabs can be machined directly into the mirror.

Typically, high-quality two-mirror imaging systems need mirror figure errors better than 1/8 of a wavelength (where one wavelength = 632.8 nm). Nickel plating was applied to the entire mirror (front, sides, and back) to counterbalance stresses induced by mismatched thermal expansion coefficients of the nickel and aluminum. Before polishing, the metal mirrors were thermally cycled repeatedly through extreme temperatures to relieve internal stresses, thereby allowing figure accuracy to be maintained over the UVISI temperature range.

Each mirror and its integral mounting tabs had to be carefully designed to maintain alignment, survive launch vibrations, and avoid stressing that could result in a distorted figure. A detailed finite-element model confirmed that extraordinary care would be required to mount and hold the mirrors without distortion. Centering posts with tight tolerances provided the alignment of the mirrors on their mounts. The machined tabs were fastened to mounting pads in the mounts with screws. Both the tabs and the pads on the mirror mount were machined and polished to ensure that the mounting surfaces did not transmit stresses to distort the mirror surface. Finally, the mounting tabs and pads were drilled and pinned to prevent slippage during launch.

Detection of faint objects requires high optical throughput, stringent rejection of stray light (mainly from the Sun), and out-of-spectral-band emissions. Degradation of optical efficiency due to hydrocarbon contamination is a particular concern in the far ultraviolet; we therefore used low outgassing materials with thorough thermal-vacuum bakeout. To reject stray light, the goal was to maintain level 300 cleanliness (a particle cleanliness standard stated for a particular particle density-size distribution slope) of critical optical components. The rejection of out-of-spectral-band radiation dictated the stringent optical filter design requirements.

Narrow-FOV Imagers

The two narrow-FOV imagers (visible and ultraviolet) have reflective telescopes with nearly identical optical and mechanical designs (Fig. 6). A two-mirror Cassegrain telescope system was chosen for the narrow-FOV design. The primary mirror is a concave paraboloid, and the secondary mirror is a convex hyperboloid. This compact reflective optical system supplies the degrees of design freedom sufficient to correct aberrations for adequate image quality over the narrow FOV. The layout also provides a substantial back focal distance to accommodate the filter wheel assembly behind the primary mirror.

UVISI requires 0.1 mrad angular resolution across the $1.3 \times 1.6°$ FOV. The FOV is mapped onto a flat
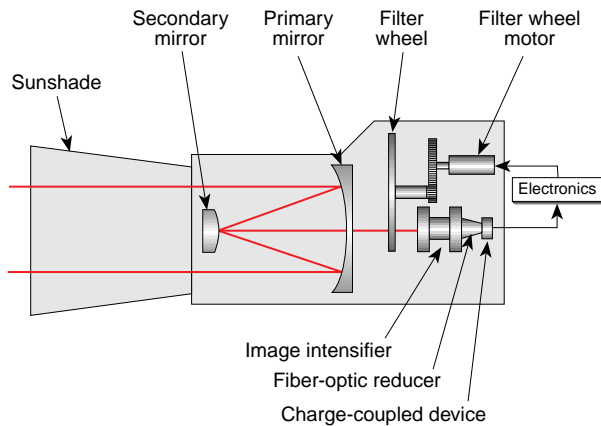
Figure 6. Optical layout of the narrow-FOV imagers.

40-mm-dia. image intensifier within the FPU; the intensifier is then coupled via fiber-optic taper to a charge-coupled device (CCD) detector. The image format of the FPU together with the FOV resulted in an effective focal length of 1350 mm. For appropriate sensitivity, a collecting area exceeding 100 cm^2 was required; the final design provides 130 cm^2.

The telescope tube consists of a cylindrical housing containing the Cassegrain mirrors and two mounting brackets. The brackets are designed to be attached directly to the MSX instrument pallet. The rear bracket holds the primary mirror along with a baffle tube and is also used for centering the mirror. The forward bracket holds the cylindrical housing in which the secondary mirror is maintained on a spider support. The sunshade assembly is mounted to the forward bracket. A conical adapter section attaches the primary mirror bracket to the filter wheel assembly. Finally, the FPU is mounted with a mechanical focus spacer to the filter wheel housing. The telescope structure with optics is about 40.6 × 17.8 × 17.8 cm and weighs 4.8 kg; an assembled narrow-FOV imager weighs 15.2 kg and uses 6 W of power.

Imager focus is adjusted during assembly with a custom-machined spacer between the filter wheel and the FPU. Boresight alignment, however, is determined purely by machined tolerances, with no tilt or decenter adjustment made on either the optical elements or the FPU. Minor adjustment of imager orientation on the spacecraft is achieved with shims.

Wide-FOV Imagers

Visible Imager

The requirement for spectral coverage of the wide-FOV visible imager was 300 to 900 nm. A three-mirror design identical to that of the wide-FOV ultraviolet imager would have met all of the requirements, but substantial size and weight reductions were achievable

by using a compact refractive design with a reduced spectral coverage (Fig. 7). Unfortunately, radiation-resistant cerium-stabilized optical glass cut off around 400 to 450 nm. But since the weight savings of a refractive system are significant, the wavelength requirement for the wide-FOV visible imager was revised to 400 to 900 nm.

The five-element design offers degrees of freedom sufficient to correct geometric and chromatic aberrations to levels yielding adequate image quality over the spectral band and FOV. The design also provides an extended back focal length to accommodate the filter wheel assembly. The back focal distance requirement is determined by the narrow-field focusing lens included in one position in the filter wheel. This lens allows the imager to focus on narrow-field particles illuminated by a xenon flashlamp during certain MSX contamination experiments.

The five-element design also has 10 lens surfaces, a configuration that results in additional scattered light and some vignetting at the FOV edges. The optical system is compact, axially symmetric, and centered; in addition, all of the lens surfaces are spherical. These features offer structural, mechanical, manufacturing, alignment, and adjustment benefits. With the use of multilayered lens coatings, reflection losses at the glass surfaces are limited to less than 1% per surface. Typical single-layer coatings yield losses of about 2% per surface. Reflection losses of the five-element lens system (9.4%), together with internal transmittance of the cerium-doped glass, result in a total transmission above 500 nm of 84.6%.

The mechanical assembly consists of an aluminum tube in which all optical elements are held with retainers. Each element is located by seats and aluminum spacers at the edge of the lens. Additional spacers hold
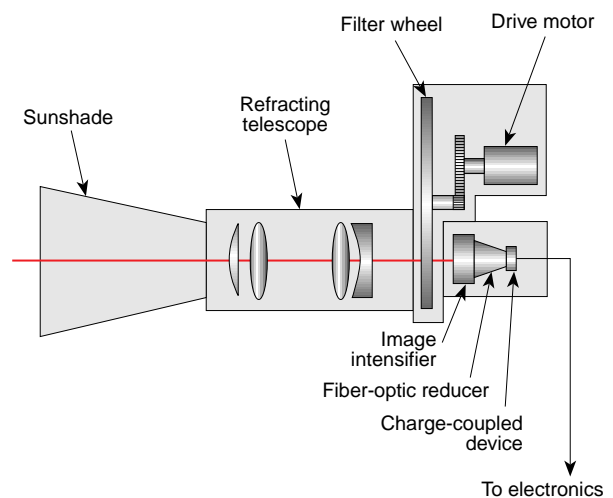

Figure 7. Optical layout of the wide-FOV visible imager.

the filter wheel assembly and the FPU. A sunshade protects the imager from stray light. Focus is adjusted with a precision-machined spacer. Boresight alignment is managed by tight mechanical tolerances on the lens seats and spacers and finally by shimming when the imager is installed on the spacecraft. The wide-FOV visible imager with optics weighs about 3.4 kg and is about 35.6 × 17.8 × 17.8 cm; with all of its components it weighs 14 kg and dissipates 6 W of power.

For a 50°C temperature change, the dimensional changes for the elements and their spacings were calculated based on the coefficient of linear expansion for aluminum (the mounting) and published coefficients of linear expansion for the glasses.[5] Changes in index of refraction with temperature shift were also calculated but were so small as to be considered negligible. Because the optical system is compact, the dimensional changes of the elements and the spacings between elements were all small enough to be neglected, except for the three largest spacings. Analysis shows that the optical system performs to specification at the cold operating temperature, even when aligned at room temperature. Good image quality was maintained when the wide-FOV visible imager was operated over the UVISI temperature range.

Ultraviolet Imager

The wide-FOV ultraviolet imager uses a three-mirror off-axis design (Fig. 8). Because transmission of these far-ultraviolet wavelengths (110–180 nm) is low in common refractive materials and the refractive materials show large dispersions in the ultraviolet band, a lens system for this imager is impractical. A reflecting system has surface powers that are invariant with wavelength and mirror reflectivities that are high across the wavelength band for better sensitivity.

The UVISI specification called for a 0.1° angular resolution for infinitely distant objects across a FOV mapped to a flat, 40-mm-dia. image intensifier in the FPU. As in the other imagers, the intensified FPU image is coupled via a fiber-optic reducing bundle to a CCD detector. To accommodate vignetting difficulties, a 14° field was mapped to the 40-mm-dia. intensifier, making the system's focal length 163 mm. The resulting FOV on the CCD detector is 10.5 × 13.1°. A collecting area of 25 cm² was required, given scene brightness, system resolution, mirror reflectivity, and detector efficiency.

The three-mirror design minimizes the number of optical components while still allowing the designer the degrees of freedom necessary to correct geometrical aberrations to provide adequate image quality over the FOV. The off-axis nature of this particular design is inefficient in its use of volume and requires large optics, but with only one aspherical element, it offers significant alignment and manufacturing advantages over other such designs with more complex mirror figures.
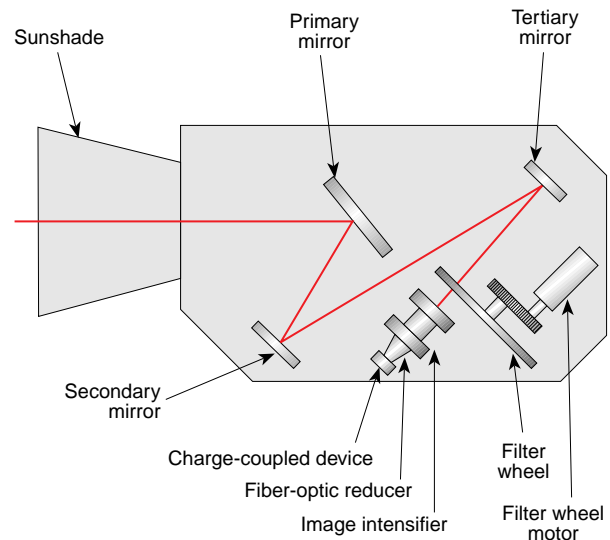

Figure 8. Optical layout of the wide-FOV ultraviolet imager.

The primary mirror is a convex sphere that reflects light to an off-axis concave ellipsoidal secondary mirror and then to a concave spherical tertiary mirror. From the tertiary mirror, the light is focused through the spectral filter housed in the filter wheel to an image on the FPU image intensifier.

The three-mirror design also causes the resulting image to be left-handed in this imager as opposed to the right-handed images in the other three UVISI imagers (i.e., left–right reversed). However, this difference is corrected in the image processing software. Because of the off-axis nature of the design, the FOV also has a small amount of keystone distortion.

The mechanical assembly consists of an aluminum honeycomb plate on which the optical elements are mounted. Each mirror is mounted to its own aluminum bracket, which is attached to the honeycomb. Additional structural pieces hold the filter wheel assembly and some interior light baffles. The FPU is mounted to the bracket holding the filter wheel housing. A sheet metal cover seals the imager from stray light. This imager is 63.5 × 53.3 × 22.9 cm and dissipates 6 W of power. The housing/optics assembly weighs 12.1 kg; the complete sensor (including FPU, SEU, and sunshade) weighs 22.5 kg.

Focus and alignment of the wide-FOV ultraviolet imager are accomplished primarily through adjustment of the tertiary mirror. The bracket for this mirror is designed for two-angle (tip and tilt) adjustment and includes a translation for focus.

Like the other imagers, the choice of an all-aluminum design eliminated effects of bulk thermal expansion, but thermal gradients across the imager could have caused misalignments. Therefore, tolerance budgeting also set limits on the thermal gradients across the imager and across the spacecraft to which it was mounted.

SENSOR SUPPORT ELECTRONICS AND HARDWARE

Focal Plane Unit

Each of the nine UVISI sensors has its own detector packaged in the FPU (Fig. 9), which performs wavelength as well as photonic-to-electrical conversion, digitizes and buffers the signal, and transmits the signal to the SEU for further processing. The FPUs contain a high-gain image intensifier tube with its associated high-voltage power supply, a frame transfer CCD, a fiber-optic taper that optically couples the image intensifier to the CCD, a 12-bit analog-to-digital converter, and the analog and timing electronics required for the CCD. All nine FPUs are of identical mechanical and electronic design, except

Figure 9. The focal plane unit.

for the photocathode material, which is selected for the appropriate band. The assemblies weigh about 2.5 kg, dissipate 2.5 W of power, and measure $17.8 \times 7.6 \times 16.5$ cm.

The FPU design and components were developed to meet several requirements. Two-dimensional imaging at reasonably high photon rates dictated the use of an integrating area detector such as a CCD. The need for minimum image smearing and antiblooming resulted in using a CCD originally designed for television rather than a full-frame CCD. The selection of the Thomson TH7866, a 550×244 pixel device, was based on the need for a medium-resolution, high-reliability part qualifiable for space use, with guaranteed operating performance. The actual resolution was reduced to 275×244 pixels by on-chip summing. This reduction was driven primarily by the required spatial and spectral resolutions, the desire for nearly square pixels, and data rate and analog-to-digital conversion time constraints. The Thomson TH7866 has shown excellent performance and operates at a fixed-gain and antiblooming control setting. The frame rate is selectable at 2 or 4 Hz, 2 Hz being the normal value.

The requirement for photon counting and a common design to cover the wide wavelength range dictated the use of an image intensifier prior to the CCD. The FPUs had to be sensitive over a 40-mm-dia. image zone determined by the optical design of both the UVISI imagers and spectrographic imagers. To meet the photon counting requirement, as well as the need to measure the pulse height distribution, we chose a high maximum electron gain of 10^6 for the image intensifier.
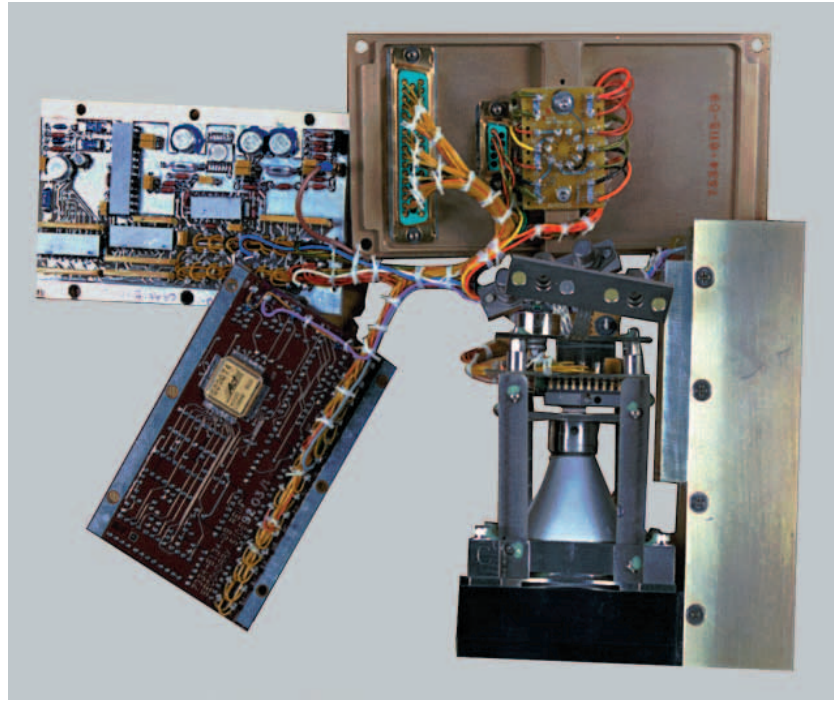
The design incorporated double-thickness 40-mm microchannel plates in a chevron configuration to obtain this gain and meet the focal plane size requirement.

The need for a common design over a wide bandpass was met by the selection of different cathode and window types. Four different cathodes—cesium iodide, rubidium telluride, bialkali, and multialkali (extended S20 type)—were chosen (see Tables 1 and 2). The first two photocathodes were deposited on magnesium fluoride windows and the last two on quartz windows. The maximum sensitivity of the FPUs is limited by cathode efficiency and statistical noise. The cathodes have a spatial uniformity of $\pm 20\%$.

The interscene dynamic range was to be as large as possible. Consequently, adjustable electron gain and gating (electronic shuttering) of the photocathode were provided. These functions are implemented in the high-voltage power supply by adjusting the voltage across the microchannel plates and by duty-cycling the photocathode voltage, respectively. The total interscene dynamic range achievable through adjustments of the gain and gating is about 10^5.

The MSX mission lifetime requirement of 4 years, with a 5-year goal, was a design driver for the image intensifier. Image intensifier lifetime is limited by the total amount of charge drawn through the microchannel plates. On the basis of a model of the expected scenes and experiments, we determined that the image intensifier had to be able to provide a 1-coulomb output charge while remaining within the cathode quantum efficiency and uniformity requirements. This performance was verified on a prototype image intensifier by

the manufacturer. To protect the image intensifier, the high-voltage power supply will be shut down if either the phosphor current exceeds 500 nA (overcurrent) or if the gain control algorithm continues to request a lower gain while the gain is at the lowest setting (algorithm peg).

The photocathodes were selected because of their sensitivity to certain wavelength ranges. They produce photoelectrons, which are amplified in the microchannel plates and electrostatically focused onto a phosphor screen, thus producing green light. This process is the wavelength translation referred to earlier. The phosphor screen is fiber-optically coupled to the CCD, which produces charge in the appropriate pixels proportional to the intensity of the light (photonic-to-electrical conversion). The coupling medium between the image intensifier and CCD is the fiber-optic taper needed to interface the different physical sizes of the image intensifier (40-mm dia.) and the CCD (8.8×6.6 mm). A fiber-optic taper was selected for this purpose instead of a lens system because of its compactness, robustness, and mass. The taper ratio of 4.55:1 was at the limit of ratios that could be produced, and in practice some distortion had to be accepted. Distortions were not in the form of spatial discontinuities but rather consisted of barrel distortion and different magnifications in orthogonal directions. Radiation-hardened glass could not be used for the fiber-optic taper. Since most of the potential radiation damage would occur at the edges of the image, several of the fiber-optic tapers were oversized so that the unused outer portion acted as a radiation shield for the active core. Any degradation at the image edge can be overcome by increasing the gain.

The FPU electronics consist of a four-board set functionally divided into a CCD and an analog, digital, and relay board. The electronics incorporate correlated double sampling for noise reduction and generate the CCD and analog-to-digital timing signals via an ACTEL ACT1020 gate array. A 12-bit analog-to-digital converter was selected on the basis of the interscene dynamic range requirement and the available data rate. The actual analog-to-digital converter part type chosen was a compromise among the conflicting attributes of conversion times (156.25-kHz sample rate), power consumption, radiation tolerance, and minimum missing codes. The interscene dynamic range is determined by the analog-to-digital resolution, the number of counts per photon, the gain control algorithm, and the analog-to-digital noise. The actual interscene dynamic range is estimated at 10^3.

Sensor Electronics Unit

Each UVISI sensor has its own radiation-hardened 80C85-based local controller or SEU. The functions of the SEU include CCD and analog-to-digital timing control; image intensifier gain control; filter wheel, scan mirror, and slit wheel mechanism control; command and telemetry communications with the DCS; data collection from the FPU; and secondary power generation and distribution to the FPUs and mechanism controllers. The SEU also buffers and inserts the bad pixel mask, generates a synchronization signal for the contamination instrument, buffers the cover open/close telltale, and provides a test port to insert known data for end-to-end digital data path verification. We opted for the use of distributed rather than centralized processing because of the large processing and input/output requirements and the need to send 12-bit parallel data across a 5-m path, which would have increased the harness weight. In addition, we wanted to provide distributed power to each sensor, with its resulting graceful degradation and overall reliability advantage.

The nine SEUs are packaged in two different mechanical housing designs to accommodate the various sensor designs. One housing mounts directly to the imager instrument pallets and the other mounts on the rear top surface of the spectrographic imagers. The SEUs have a nearly identical electrical design implemented on two "rigid-flex" multilayered printed circuit boards. The only differences electrically among the nine units are the contents of a single programmable read-only memory (PROM) on each unit, which contains sensor-specific parameters (e.g., maximum gain and gain offset for the image intensifiers), and the stepper motor phase at a reference position for each mechanism. All SEUs weigh about 2.4 kg, dissipate 2.8 W of power, and measure $21.6 \times 17.8 \times 7.9$ cm.

The SEU controls the CCD sequencer timing and can read out the CCDs at a commandable 2- or 4-Hz frame rate. To maintain a constant data rate at both 2 and 4 Hz, the imager FOV is reduced by about 60% in the 4-Hz mode. Twelve-bit parallel image pixel data are transferred from the FPU to the SEU at 156.25 kHz.

Known bad pixels are masked per the bad pixel map, which is stored in the DCS electrically erasable PROM (EEPROM) and uploaded to each SEU. Masking, if invoked, involves replacing the current pixel by zero or the last valid pixel. The data are then sent to both the gain control logic and to the DCS.

The image intensifier gain control parameters are selectable, thus allowing the experimenter the ability to optimize each sensor's science data. The image intensifier gain is the product of the microchannel plate gain and the image intensifier duty cycle. The SEU drives an 8-bit digital-to-analog converter in the FPU, which controls the microchannel plate's high-voltage output (microchannel plate gain) and provides a signal that gates the photocathode voltage "on" or "off," effectively controlling the image intensifier duty cycle. The maximum integration time for the 2-Hz mode is

468 ms. The duty cycle can be controlled over a range of 0.24 to 100% of full scale, with a resolution of 0.48%. Microchannel plate gain and gate combinations are defined in gain tables. Several predefined gain tables are stored in memory.

A nominal microchannel plate gain versus voltage curve was determined from the image intensifier transfer functions provided by the manufacturer. Since each gain curve varies from the nominal, maximum voltage and offset values were determined for each tube to normalize the tube response. To determine which step in the table is appropriate for a given scene, the SEU forms a histogram of the analog-to-digital converter output and compares it with the exposure rules. An ACTEL 1020 field-programmable gate array bins pixel values and compares them with preset threshold values in real time. When the maximum allowable number of pixels fall outside the range of programmed upper or lower limits, the SEU moves a software pointer downward or upward in the preselected gain table to pick a new combination of gain and gate values to send to the FPU image intensifier. Gain adjustments are calculated on data from the previous frame and applied to the next frame. Therefore, an inherent one-frame time delay in the gain control algorithm exists. To avoid instability, the gain is corrected every other frame.

Four thresholds are defined: saturation, upper, lower, and subthreshold. When the number of pixels exceeds the allowable saturation threshold or is under the subthreshold, the gain is dropped or increased by a large step in the gain control table. When the number exceeds the allowable upper or lower thresholds (but not the saturation or subthresholds), the gain is dropped or increased by a small step in the gain control table. Several gain tables are available, and new tables can be uploaded. The gain control mode, table, saturation and subthresholds, number of pixels allowed to exceed each threshold, and step sizes are all commandable. Upper and lower thresholds are defined by the table selected.

Image intensifier gain control is available in five different modes: automatic, manual, absolute, calibrate, and mirror lock. The automatic mode is the nominal gain control mode described earlier. In the manual mode, the initial index in the table is commanded, and the gain is only permitted to decrease from that point. In the absolute mode, the actual microchannel plate gain and gate values are specified. This mode does not use the tables; therefore, the maximum gain and offset values are not applied. The microchannel plate gain is decreased if saturation occurs. The absolute mode was used extensively for ground calibration and is not recommended for flight. In the calibrate mode, the gain gradually ramps up to a maximum value and ramps back down again. This mode will be used extensively for in-flight calibration. Maximum gain, step size, dwell time in frames, and table start index are all commandable

options in the calibrate mode, as is the decision to go up and down or just up. Finally, the mirror lock mode calculates the gain based on the data from a specific scan mirror position while a SPIM is scanning. This mode is required because the target is not necessarily in the FOV throughout the scan.

The SEU controls the scan mirror, slit, and filter wheel motors by driving the stepper motor windings through an output port. The slit and filter wheel motors operate in single phase, whereas the scan mirror motor operates in dual phase. To damp mirror position ringing, the last phase in scan mirror movement is held energized for 25 ms after the move is complete. The SEU also receives fiducial position feedback information from each mechanism.

Communications between the DCS and SEU involve both high-speed data and low-speed command/status interfaces. The data are sent from the SEU to the DCS synchronously with the 156.25-kHz FPU data collection rate on a serial interface clocked at 2.5 MHz. The sensor data and the bad pixel mask are sent serially to and from the DCS via differential driver/receiver pairs, respectively. The command/status interfaces are implemented using low-speed opto-couplers and universal asynchronous receiver transmitter (UART) integrated circuits. Commands received by the SEU from the DCS are echoed back for verification and then decoded by the SEU into specific sensor control functions. A new command is received and decoded at the beginning of either a 2- or 4-Hz integration period to initiate the transition of the SEU control registers and hardware flags on the next frame synchronization signal before the start of the next integration period. Sensor status or housekeeping data are updated every frame so that there is minimum delay between new command execution and sensor status output resulting from that command. Sensor status provides information such as imager filter wheel or spectrograph slit wheel and scan mirror positions, video gain control modes, bad pixel masking modes, and image intensifier gain and gating values. Each SEU can communicate with each of the redundant DCSs.

To provide flexibility and conserve power, the sensors can be individually powered via solid-state relays located in the DCSC. Each SEU houses a DC/DC converter, which provides ±5 and +15 V to the FPU and +5 V to the SEU itself.

Finally, to independently verify the digital data path (SEU through DCS to the data handling system [DHS] or the image processor), one can insert known test patterns into the SEU test port and compare them with the output of the DCS for each telemetry mode.

Sunshades/Covers

Each sensor has an aluminum light baffle or sunshade to reject stray light entering the optical path. The

sunshades, which include knife-edge baffles, were milled out of two pieces of aluminum. An epoxy-based spacer was added between the two sections to thermally isolate the sunshade from the sensor housing. Interior surfaces were treated with Martin Black, a proprietary flat black coating, to minimize off-axis reflection.

Each sunshade is equipped with a one-time open cover to protect the optics from particulate contamination through launch. The cover mechanism design involves a latch and a spring-loaded hinge. The latch is held in place by a detent spring and is released via redundant bellows motors (pyros). The cover is designed to open beyond a 180° angle to prevent glint from entering the FOV. Each cover has a 50.8-mm-dia. window and attachment points to mount an external lamp/telescope assembly for end-to-end optical testing of the system.

INSTRUMENT SUPPORT ELECTRONICS

Data Control System

The DCS is the single interface for the operation of all nine UVISI sensors via the spacecraft command and data handling systems, and the UVISI imagers interface via the image processor. It is one of two redundant packages in the instrument. The DCS commands the sensor's operational mode and its on and off sequence. It is designed to process the sensor data to match the bandwidth of the sensors to the available spacecraft telemetry bandwidth on the 16-kbps, 1-Mbps, and prime-science 5- or 25-Mbps telemetry links. This subsystem synchronizes all sensor data collection in either the 2- or 4-Hz frame rates.

The DCS selects one, two, or four imagers for output in the prime-science telemetry, one of four imagers for output in the wideband telemetry, and one of four imagers for output to the image processor. It can be commanded to compress 12 (nonintegrated) or 16 (integrated) bits/pixel to 8 bits/pixel for output. For the SPIMs, the DCS can perform selectable two-dimensional pixel integration with options of 272, 136, or 68 pixels per line in the spectral dimension and 40, 20, 10, or 5 lines per frame in the spatial dimension. It also supports the MSX Contamination Experiment by synchronizing the gating of the SPIM 3 and the wide-FOV visible imager FPUs to the flashing of the krypton and xenon lamps when required. Figure 10 illustrates the DCS system interface.

Each DCS comprises nine different circuit boards plus a motherboard. The circuit boards were built using a stitch-weld process; the interconnections on each 19.6 × 18.8 cm board are made with Teflon polyimide overcoated solid nickel wire welded to studs mounted in the board. The motherboard provides the electrical
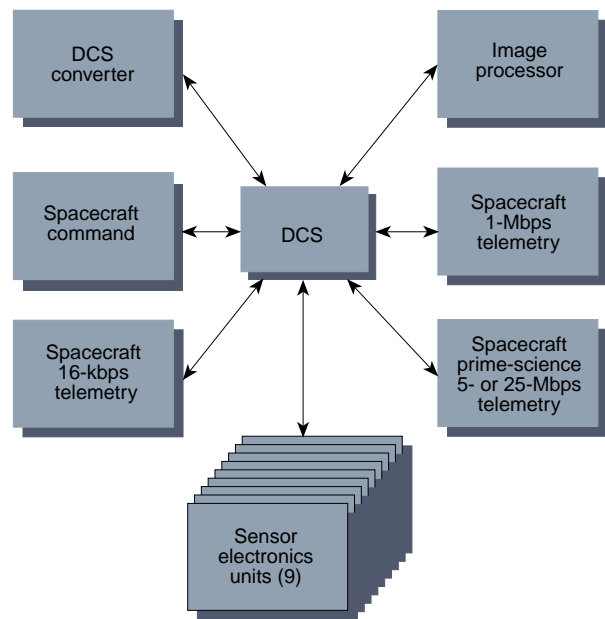

Figure 10. Data control system interfaces.

interconnections between the subsystem boards. Each electronics package measures about 53.3 × 27.9 × 20.3 cm, weighs 8.6 kg, and dissipates 11 W of power.

DCS Instrument Control Processor

The DCS instrument control processor decodes the commands and configures the DCS data processing and telemetry output. It is based on the 80C85RH 8-bit microprocessor. The instrument control processor software is contained in PROM. EEPROM adds the ability to upload software changes while in orbit. A pair of serial interfaces receives commands from either of the redundant MSX command systems. Macro commands stored in either PROM or EEPROM are used to minimize the number of commands needed from the spacecraft. A single macro command can trigger any desired combination of DCS or sensor commands. The use of macro commands simplifies ground operation of the UVISI system and automates a variety of functions, including initialization and shutdown of the sensors.

The sensors use UART links to output status data to the instrument control processor, which combines these data with its own status data and transmits all the data to the MSX DHS on a serial interface for inclusion in the spacecraft's housekeeping telemetry.

Imager status data are also transmitted on a parallel interface to the UVISI image processor for use in its processing algorithms. The instrument control processor also accepts a limited number of commands from the image processor on a parallel interface. The image processor is allowed to select the imager to be processed, as well as the gain control mode and the filter wheel position of that imager.

DCS Spectrograph Data Processing Electronics

The DCS spectrograph data processing electronics transmit frame synchronization, clocks, and bad pixel masking signals to the spectrographs and receive 2.5-MHz serial pixel data. The serial data are converted to 12-bit parallel data and multiplexed through a two-dimensional pixel integrator. The integrator is commandable by the instrument control processor to sum the spectrograph data both spectrally and spatially. The data are then passed through an optional data compression function that can be commanded to compress 12-bit (nonintegrated) or 16-bit (integrated) data to 8 bits. Pixel integration and data compression can be used to obtain a variety of different spectrograph data bandwidths to meet varying mission requirements. The processed data are stored in random access memory (RAM) and are made available to the DCS prime-science telemetry formatter for output in the MSX prime-science telemetry.

DCS Imager Data Processing Electronics

The DCS imager data processing electronics transmit frame synchronization, clocks, and bad pixel masking signals to the imager and receive 2.5-MHz serial pixel data. The serial data are converted to 12-bit parallel data, and, by instrument control processor command, the data from one, two, or four of the imagers are multiplexed into a selectable data compression function that can compress the 12-bit data to 8 bits. Data compression and selection of only the required imagers can be used to obtain a variety of imager data bandwidths. The processed data are stored in RAM and are made available to the prime-science telemetry formatter for output in the MSX prime-science telemetry. One of the four imager data streams is captured in a separate RAM and is made available to the DCS wideband telemetry formatter for output in the MSX wideband telemetry.

The DCS imager data processing electronics also interface to the UVISI image processor. One of the four imager serial data streams is broadcast to the UVISI image processor under control of the instrument control processor. The image processor also outputs processed images to the DCS for inclusion in both the MSX prime-science telemetry and the MSX wideband telemetry. These data are buffered in first-in/first-out buffers until used by the DCS telemetry formatters.

DCS Wideband Telemetry Formatter

The DCS wideband telemetry formatter accepts buffered imager and image processor data for output in a variety of formats under the control of the instrument control processor. The wideband telemetry interface to the spacecraft is a 1-MHz serial link used for real-time observations. MSX allows UVISI two different data bandwidths, depending on mission requirements. At the higher bandwidth setting (911 kbps), the imager and image processor data are output each data frame. At the lower bandwidth setting (232 kbps), the imager data are output only every fifth frame.

DCS Prime-Science Telemetry Formatter

The DCS prime-science telemetry formatter accepts buffered imager, spectrograph, image processor, and instrument control processor status data for output in a variety of formats. The prime-science telemetry interface to the spacecraft is a 2.5-MHz serial link used for recording observations for later playback to the MSX ground station. MSX allows UVISI three different data bandwidths from 1.13 to 5.85 Mbps depending on mission requirements. The DCS uses the capabilities of the spectrograph data processing electronics and the imager data processing electronics to reduce the sensor data bandwidth to that allowed by the mission requirements. The DCS prime-science telemetry formatter also synchronizes the entire UVISI instrument by locking onto a 1-pulse-per-second signal and a 5-MHz clock provided by the spacecraft. By locking the UVISI sensors to the MSX DHS, data time-tagging requirements are minimized.

Data Control System Converter

The DCSC is located adjacent to the DCS on the spacecraft electronics pallet. Its redundant three-board electronic design, cross-strapped to the DCS, resides within one 22.9 × 22.9 × 20.3 cm structure. It weighs 2.5 kg and dissipates 8.6 W of power. The DCSC houses the DC/DC converters and power switching relays for the redundant DCSs, which each receive +5 and −5.2 V. Solid-state relays, which feature an integrated circuit breaker, are used to switch power to each UVISI sensor. The relays are controlled by a parallel interface to the DCS instrument control processor.

Imager Processor

The UVISI instrument contains an image processor that selects and processes images from one of the four imaging sensors. Its purpose is to provide the spacecraft tracking processor with information needed to complete closed-loop tracking of targets of interest.[8] From an analysis of the contents of each image, the image processor generates a list of potential targets. This list is sent to the MSX tracking processor, where its data are input to a tracking loop. The image processing algorithms executed by the image processor are largely software-based and can be changed by uploading new software.

Overall control of the image processor and image processing is performed by a MIL-STD-1750A processor programmed in Ada. The 1750A processor addresses 512 KB of RAM, which has an error detection and correction function, and 256 KB of EEPROM. The bulk of the image processing is performed in a digital signal processor that runs under the control of the 1750A processor. The digital signal processor is based on a 2100 digital signal processing chip and can address a total of 366 KB of RAM on two buses; the RAM contains code, stored images, and coefficients. Code for both 1750A and DSP-2100 is stored in EEPROM. When the image processor is powered up, code for both processors is transferred from EEPROM to RAM prior to execution. Any one of the four available imagers may be selected and used for tracking; onboard control logic and ground commands determine which imager is used as well as the criteria for switching from one imager to another. An interface to the MSX DHS via the instrument DCS allows the DHS to collect serial digital housekeeping telemetry data from the processor. The processor electronics design weighs 8.6 kg, including the DC/DC converter, and requires 10 W of power. It is packaged in a chassis that measures 31.8 × 23.9 × 9.5 cm. The unit contains six multilayered printed circuit daughterboards that use surface-mount technology and one multilayered motherboard. Four of the daughterboards are common with spacecraft attitude and tracking processor designs. (For a comprehensive discussion of UVISI image processing, see Ref. 9.)

Software

The main requirements for UVISI software development were established early in the program. UVISI control software (DCS and SEUs) is designed to manage the low-level functions of the instrument that perform operations required to command and control it.[10] In addition to the many low-level functions noted throughout the article, there are several features built-in for ease of use, flexibility, and troubleshooting. For example, EEPROM is used in the DCSs to update parameters, gain control tables, bad pixel mask tables, etc. Over 100 macro commands are also built into EEPROM for often-used command strings. Finally, to aid in troubleshooting, the software incorporates autonomy, failure modes for each of the mechanisms, automatic shutdown of the image intensifiers, several diagnostic telemetry modes, and a memory dump mode. Three separate control programs have been developed: the instrument control processor in the DCS, the imager control processor in the imager SEU, and the spectrograph control processor in the SPIM SEU. These are all 8085-based hosts and are programmed in C and assembly language.

The image processor is composed of a specially designed preprocessor board used for subimage selection, the Analog Devices digital signal processor ADSP-2100 radiation-hardened board for fast vector processing, and a 1750 microprocessor to perform nonvectorized processing. Most of the flight software is programmed in Ada; low-level routines are coded in assembly language. Both processors can be reprogrammed in orbit.[9]

SUMMARY

The UVISI instrument consists of five spectrographic imagers, four imagers, and their support electronics that together provide spectra and image data from the far ultraviolet to the near infrared. It was designed to research a variety of celestial, atmospheric, and point sources for military, scientific, and environmental investigations over a planned 4-year lifetime.

The instrument has completed its integration, environmental qualification, and calibration phases and has been delivered to the MSX spacecraft for launch.

REFERENCES

[1]Paxton, L. J., Meng, C.-I., Anderson, D. E., and Romick, G. J., "MSX—A Multiuse Space Experiment," *Johns Hopkins APL Tech. Dig.* **17**(1), 19–34 (1996).
[2]Carbary, J. F., Darlington, E. H., Harris, T. J., McEvaddy, P. J., Mayr, M. J., et al., "Ultraviolet and Visible Imaging and Spectrographic Imaging Instrument," *Appl. Opt.* **33**(19), 4201–4213 (1994).
[3]Peacock, K., "Design and Calibration of the MSX-UVISI Spectrographs," in *Proc. International Workshop on VUV and X-Ray Radiometry for Space-Based Instruments*, Berlin, Germany, pp. 77–80 (1994).
[4]Maurer, R. H., *Radiation Total Dose Levels for UVISI*, JHU/APL SOR-5-90031 (19 Feb 1990).
[5]Pellicori, S. F., Russell, E. E., and Watts, L. A., "Radiation Induced Transmission Loss in Optical Materials," *Appl. Opt.* **18**(15), 2618–2621 (1979).
[6]Duncan, D. D., and Cotter, T. M., *Radiation Damage to Optical Glasses and Fibers*, JHU/APL F1F(4)90-U-002 (2 Jan 1990).
[7]*Radiation Resistant Optical Glasses (Cerium Stabilized)*, Schott Report 7600e-1975, Mainz, West Germany (1975).
[8]Garlick, D. S., Malcom, H., and Murphy, P. K., *UVISI Image Processor Software Detail Design Document*, JHU/APL S1A-036-91 (12 Apr 1991).
[9]Murphy, P. K., and Heyler, G. A., "Image Processing Aboard the Midcourse Space Experiment Using the Ultraviolet and Visible Imagers and Spectrographic Imagers Instrument," *Johns Hopkins APL Tech. Dig.* **15**(3), 195–205 (1994).
[10]Hook, B. J., and Garlick, D. S., *Midcourse Space Experiment UVISI Intrument Control Software Design Document Version 3.0*, JHU/APL S1A-244-93 (1 Oct 1993).

THE AUTHORS

KEVIN J. HEFFERNAN is a member of APL's Principal Professional Staff and supervisor of the Systems Engineering Section of the Space Instrumentation Group. He received a B.S.E.E. degree from Drexel University in 1975 and an M.S.E.E. from The Johns Hopkins University in 1980. Since joining the Laboratory in 1977, Mr. Heffernan performed digital design and systems engineering work almost exclusively for space instrumentation programs. He was the systems engineer for both the Hopkins Ultraviolet Telescope and the UVISI instrument, and is currently serving as the instrument systems engineer for the Thermosphere-Ionosphere-Mesosphere Energetics and Dynamics program. Mr. Heffernan is a member of the American Institute of Aeronautics and Astronautics and the Society of Photo-optical Instrumentation Engineers. His e-mail address is Kevin.Heffernan@jhuapl.edu.
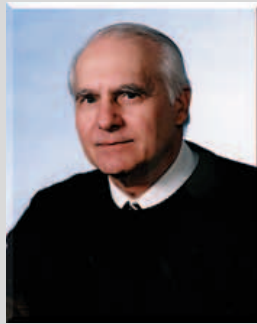
JOHN E. HEISS received his B.S. degree in electrical engineering from the Illinois Institute of Technology and attended The Johns Hopkins University McCoy College, where he studied industrial management. He is the UVISI program manager for the MSX Program Office. Mr. Heiss became a member of the Senior Professional Staff of APL's Space Department in 1972 and was assigned to the Reliability and Quality Assurance Group as a product assurance performance engineer. He was subsequently appointed supervisor of the Quality Assurance Section. During the last 8 years, Mr. Heiss has worked in the Space Department's Program Management Office on five different spacecraft and four scientific instruments in addition to developing quality policy and practices for the Department. His e-mail address is John.Heiss@jhuapl.edu.

JOHN D. BOLDT is a member of the Space Sciences Instrumentation Group. Since joining APL in 1982, he has worked on spacecraft power systems and mission operations in addition to his current work with data systems for scientific instruments. He has designed data systems for the U1, U2, and U3 instruments flown on the Delta 180, 181, and 183 missions as well as a processor system used by instruments on the Near Earth Asteroid Rendezvous and Advanced Composition Explorer spacecraft. His e-mail address is John.Boldt@jhuapl.edu.

E. HUGO DARLINGTON received a B.Sc. (Hons.) degree from Durham University and a Ph.D. from the Cavendish Laboratory, Cambridge, England, and is a Chartered Engineer. He has worked in electron physics and elemental analysis and also has experience in electron, ion, light, and ultrasound optics. For the last several years, he has been developing optical sensors for space-based instruments. Dr. Darlington is a member of the APL Principal Professional Staff and the Space Sciences Instrumentation Group. He teaches courses in electronics and optical radiation detectors at JHU's G. W. C. Whiting School of Engineering. His e-mail address is Edward.Darlington@jhuapl.edu.

KEITH PEACOCK received a B.Sc. in physics from Durham University in 1961, an M.Sc. in radioactivity from Birmingham University in 1962, a Ph.D. in astronomy from Manchester University in 1967, and an M.S. in technical management from The Johns Hopkins University in 1984. Before coming to APL in 1979, he worked at Bendix Aerospace Systems and at the Los Alamos National Laboratory. During his first 8 years at APL, he worked on the Submarine Security Program, then joined the Space Instrumentation Group in 1988. He received two Lawrence Hafstad Fellowships for work on optical design projects in JHU's Department of Physics and Astronomy. His primary field of interest is optics; he designed the five MSX UVISI spectrographs, the Special Sensor Ultraviolet Spectrographic Imager and Global Ultraviolet Imager ultraviolet spectrographs, and the Near Earth Asteroid Rendezvous infrared spectrograph. Dr. Peacock also teaches optics at JHU's G. W. C. Whiting School of Engineering. His e-mail address is Keith.Peacock@jhuapl.edu.

TERRY J. HARRIS joined APL in 1982 and has been a member of the Electro-Optical Systems Group since 1983. He is a specialist in optical system design and analysis, stray light analysis, and geometrical optics. Mr. Harris has served as the optical designer for several space-based instruments and ground-based systems for a wide variety of applications. He has also worked in wavelengths from the ultraviolet to far infrared. His e-mail address is Terry.Harris@jhuapl.edu.

MARK J. MAYR received a B.S.E.E. degree from the Milwaukee School of Engineering in 1978 and an M.S.E.E. degree from The Johns Hopkins University in 1981. He is a member of APL's Principal Professional Staff and the supervisor of the Electro-Optical Systems Group's Guidance Evaluation Section. Since joining APL in 1978, he has worked on various projects associated with electro-optical, inertial, and control systems. Mr. Mayr led the design, fabrication, integration, and testing of the UVISI imagers, as well as the integration and testing of the UVISI spectrographic imagers. In addition, he has worked on infrared seekers for interceptor missiles, map matching systems for cruise missiles, a precision pointing and tracking system for a high-energy laser weapon, and other electro-optical instrumentation and sensor efforts. Mr. Mayr is a member of the Society of Photo-optical Instrumentation Engineers. His e-mail address is Mark.Mayr@jhuapl.edu.